

Supporting Information

Regulating electronic structure of metal–organic framework via ion-exchanged Ir dispersion for robust overall water splitting

Shunfa Zhou,^a Yuxuan Liu,^b Jiawei Shi,^a Jing Li,^a Weiwei Cai*^a

^a Sustainable Energy Laboratory, Faculty of Materials Science and Chemistry, China University of Geosciences, Wuhan, 430074, China.

E-mail: willcai1985@gmail.com; caiww@cug.edu.cn.

^b Wuhan Monitoring Station, State Urban Water Supply Quality monitoring Network, No. 240

Jiefang Avenue, 430034, Wuhan, China

Experimental

Synthesis of Co-BDC

A uniformly stable solution A was prepared by mixing 1 mmol of $\text{Co}(\text{NO}_3)_2 \cdot 6\text{H}_2\text{O}$ in 4.5 mL of N, N-dimethylformamide (DMF). Simultaneously, a solution B was prepared by taking 1 mmol of terephthalic acid and dissolving it in 7.5 mL of DMF. Subsequently, 1 mL of 0.4 M NaOH solution was added to this mixture. Then, solution A was poured into solution B. The resulting mixture was transferred into a 25 mL Teflon-sealed autoclave together with a piece of pre-treated nickel foam (NF, 1.5 cm \times 3 cm). The hydrothermal reaction was conducted at 100 °C for 15 h, and the product was then rinsed with deionized water. Finally, Co-BDC was obtained after drying at 65 °C.

Synthesis of $\text{CoIr}_x\text{-BDC}$

Certain amount (10, 20, 30 and 40 mg) of IrCl_3 was dissolved in 18 mL ethanol and a Co-BDC sheet was immersed in the IrCl_3 solution in a 25 mL Teflon-sealed autoclave for hydrothermal reaction at 80 °C for 12 h. After the reaction, the resulting blackened NF was rinsed with ethanol repeatedly. Finally, $\text{CoIr}_x\text{-BDC}$ products ($x=1, 2, 3$ and 4 with 10, 20, 30 and 40 mg IrCl_3 , respectively) were obtained after drying.

Characterizations.

The crystal phase of both freshly synthesized powders were detected by X-ray diffraction (XRD, Bruker AXS D8-Focus, Germany) with Cu $K\alpha$ radiation in the range of 2θ from 10° to 80°. The micromorphology of $\text{CoIr}_x\text{-BDC}$ and Co-BDC powders were observed by means of a field emission scanning electron microscopy (FESEM, Hitachi SU8010, Japan). The X-ray photoelectron spectroscopy (XPS, Escalab 250XI, ThermoFisher, USA) was employed to further explore the composition, chemical environment and surface electronic state of the

samples, and the atomic proportion of each element is determined by the area ratio of its characteristic peaks. All XPS profiles are aligned by C 1s (284.60 eV). The transmission electron microscope (TEM) and high-resolution transmission electron microscope (HR-TEM) images were observed under JEM-2100F field emission transmission electron microscopy. The Ir content of all samples were measured by Inductively coupled plasma mass spectrometry (ICP-MS).

Electrochemical measurements

All the electrochemical measurements were performed on a Gamry electrochemical workstation with a typical three-electrode system configuration in 1 M KOH. LSV at a scan rate of 5 mV s^{-1} was performed under 1 M KOH electrolyte using various catalysts as the working electrode, graphite rod as the counter electrode and Hg/HgO electrode as the reference electrode with iR compensation unless otherwise stated. The reference electrode, Hg/HgO was calibrated with respect to the reversible hydrogen electrode (RHE), $E_{\text{RHE}} = E_{\text{Hg/HgO}} + 0.059 \times \text{pH} + 0.099$. Operando electrochemical impedance spectroscopy (EIS) tests were performed over a frequency range from 0.05 to 10^5 Hz with AC amplitude of 10 mV. The durability of CoIr₃-BDC catalyst tested by Chronopotentiometry (CP) method for 30h.



Figure S1. Schematic illustration of the synthetic process of CoIr_x-BDC.

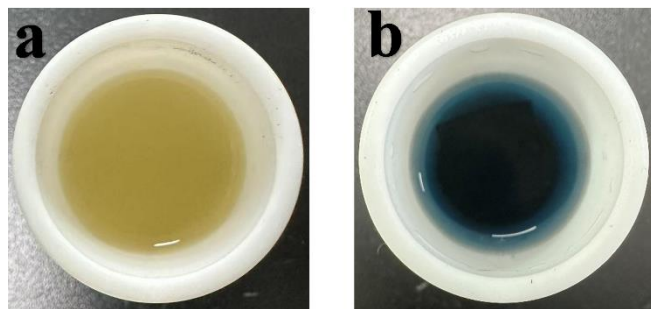


Figure S2. Optical images of solution in the pressure vessel before (a) and after (b) reaction.

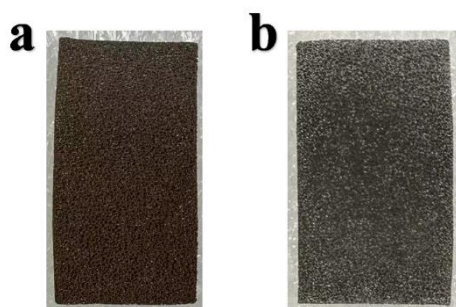


Figure S3. Optical images of Co-BDC and CoIr₃-BDC.

Photographs of the solution within the pressure vessel were captured prior to and subsequent to the reaction. The observed color change, from brown to blue, after the reaction indicates the successful substitution of partial Co sites by Ir atoms via the ion exchange process (Figure S2). Additionally, the alteration of the Co-BDC color from brown to black following the ion exchange provides supplementary evidence supporting the incorporation of Ir elements into the Co-BDC MOF materials via the ion exchange strategy (Figure S3).

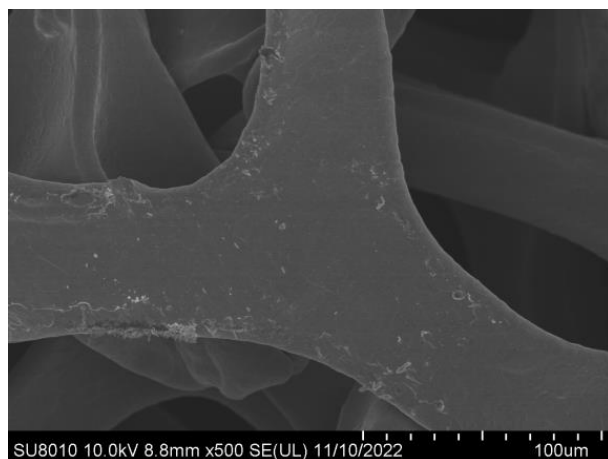


Figure S4. SEM images of bare NF.

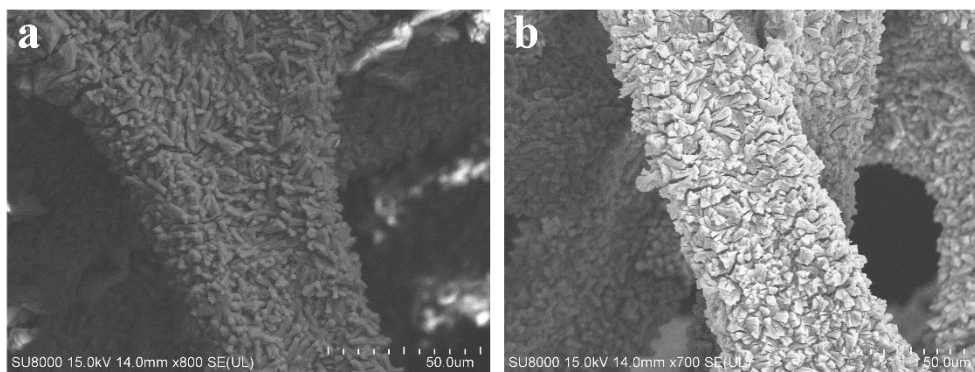


Figure S5. SEM images of Co-BDC and CoIr₃-BDC at higher magnification.

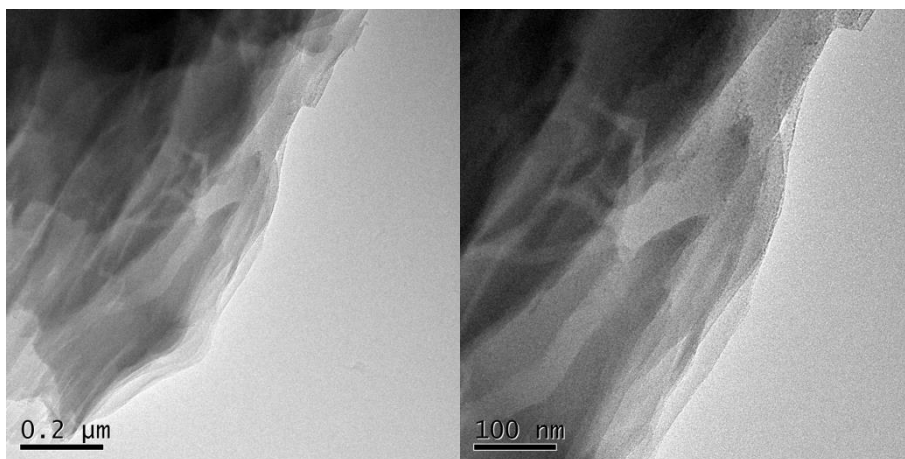


Figure S6. TEM images of CoIr₃-BDC catalyst.

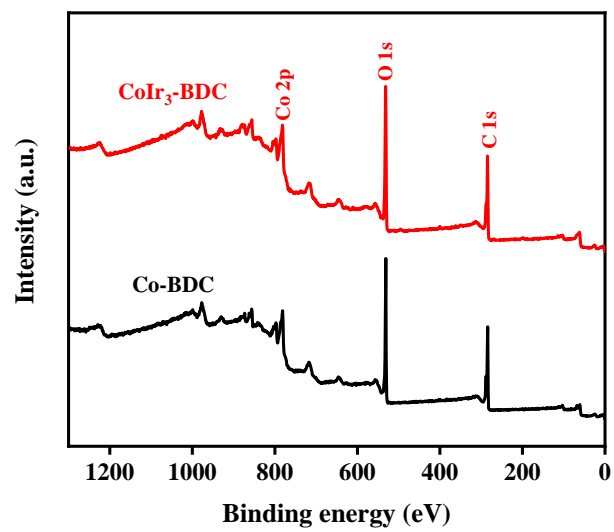


Figure S7. Survey XPS spectra of Co-BDC and CoIr₃-BDC.

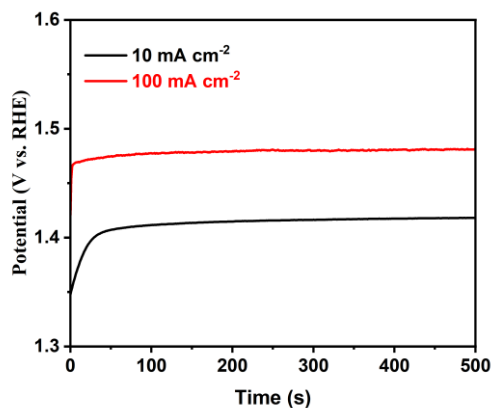


Figure S8. OER chronopotentiometry curves of CoIr₃-BDC at 10 and 100 mA cm⁻².

For the precise determination of the actual overpotential encountered during the Oxygen Evolution Reaction (OER) process, a chronopotentiometry analysis of CoIr₃-BDC was conducted at current densities of 10 and 100 mA cm⁻². This methodology was employed to address potential uncertainties arising from significant cathodic peaks observed at lower potentials in the polarization curve. The results, depicted in Figure S8, highlight the exceptional catalytic efficiency of CoIr₃-BDC, as evidenced by the corresponding η_{10} and η_{100} values of 186 and 252 mV, respectively. Importantly, these values exhibit a close resemblance to those derived from the LSV curve.

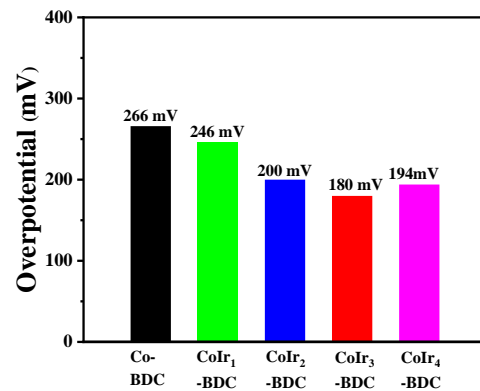


Figure S9. The OER overpotential of CoIr_x-BDC and Co-BDC catalysts to reach 10 mA cm⁻².

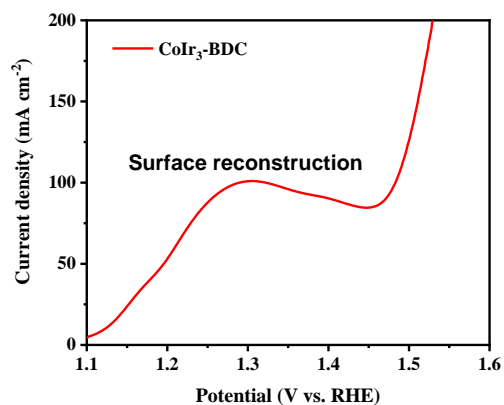


Figure S10. LSV curve of CoIr₃-BDC measured in the forward direction.

As shown in Figure S10, the LSV curve measured in the forward direction exhibits a large oxidation peak, which can be attributed to the oxidation of Co²⁺ to high-valence state Co species, indicating the surface reconstruction of CoIr₃-BDC during the OER process.

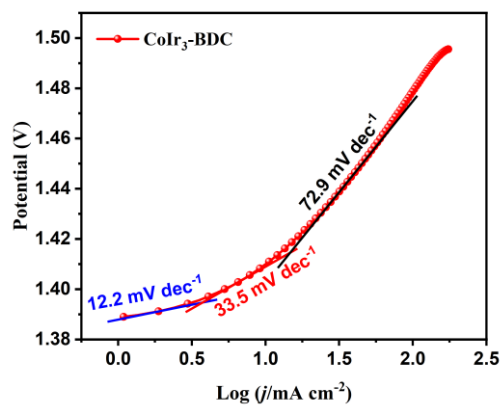


Figure S11. Tafel plots of CoIr₃-BDC with different current range.

Typically, the Tafel slope is determined within a current density range below or around 10 mA cm⁻². Therefore, we opted for a current density range around 10 mA cm⁻² to derive the Tafel slope of CoIr₃-BDC

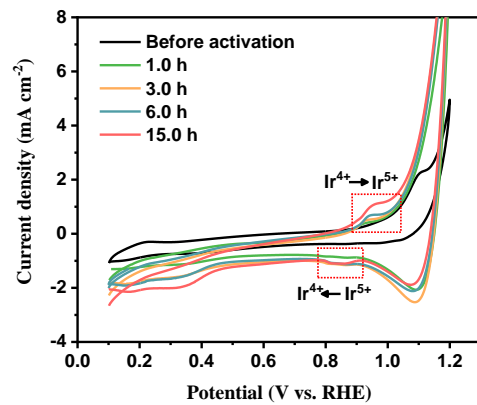


Figure S12. CV curves of CoIr₃-BDC with 10 mV/s scan rate. It was recorded before and after 1, 3, 6 and 15 h chronopotentiometric OER process.

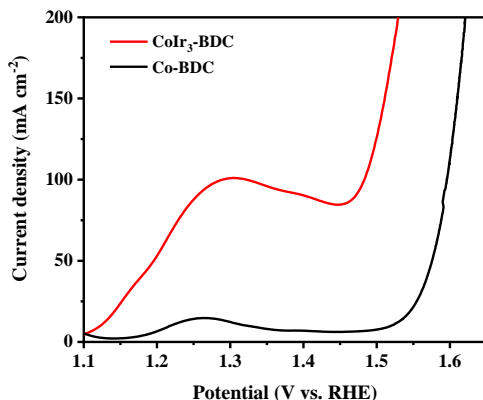


Figure S13. OER LSV curves of CoIr₃-BDC and Co-BDC.

Figure S12 shows the CV curves before and after several hours (1, 3, 6 and 15 h) of the CP test (fixed at a current of 100 mA cm⁻²). The oxidation peak at 0.95 V is attributed to the Ir⁴⁺/Ir⁵⁺ oxidation peak. The appearance of Ir⁴⁺/Ir⁵⁺ suggests that available active sites are present on the surface. This most likely originated from an increase in Ir sites with increasing OER potential or cycle number because of coordination with more O species during the OER process. Significantly, the Ir⁴⁺/Ir⁵⁺ oxidation peak emerges immediately after only 1.0 h of the CP process and shows a time-dependent current density enhancement from 1.0 to 15 h. This indicates the formation of Ir⁵⁺ species and the more pronounced surface oxidation transition of Ir⁴⁺/Ir⁵⁺ during the OER. According to the OER mechanism that involves the onset of the OER starting with Ir⁴⁺-OH becoming oxidized to Ir⁵⁺=O, the formation of Ir⁵⁺ sites is a necessary condition for the OER. Hence, the introduced Ir in CoIr₃-BDC is considered one of the active sites for the OER. The Co²⁺→Co^{3+/4+} oxidation peak is located at ~1.3 V in the CoIr₃-BDC LSV curve (Figure S13). This Co²⁺→Co^{3+/4+} oxidation peak is affected by the introducing metal cations in CoIr₃-BDC. Compared with Co-BDC, the increase in the oxidation peak of CoIr₃-BDC suggests that Co atoms become more electrochemically active after the introduction of Ir. Thus, it can be concluded that Co sites and Ir sites both serve as active sites for CoIr₃-BDC during OER process.

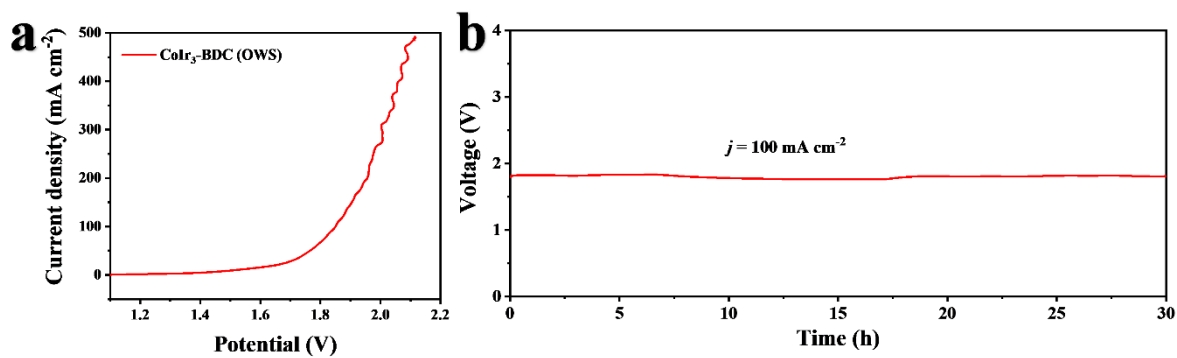


Figure S14. Overall water splitting performance. (a) LSV curves of the CoIr₃-BDC||CoIr₃-BDC in 1 M KOH without iR compensation and (b) CP curve of CoIr₃-BDC toward overall water splitting at 100 mA cm⁻².

Table S1. Ir content of CoIr_x-BDC catalysts measured by ICP-MS.

Catalyst	CoIr ₁ -BDC	CoIr ₂ -BDC	CoIr ₃ -BDC	CoIr ₄ -BDC
Ir content (wt%)	0.19%	0.23%	0.28%	0.44%